

**EFFECT OF SECONDARY PLASTIC DEFORMATION ON THE  
MICROSTRUCTURES AND MECHANICAL PROPERTIES OF  
CAST Al-7Si-Mg ALLOY**

**NGUYEN VAN THUONG**

**2014**

**EFFECT OF SECONDARY PLASTIC DEFORMATION ON THE  
MICROSTRUCTURES AND MECHANICAL PROPERTIES OF  
CAST Al-7Si-Mg ALLOY**

**by**

**NGUYEN VAN THUONG**

**Thesis submitted in fulfillment of  
the requirements for the degree  
of Master of Science**

**July 2014**

## **ACKNOWLEDGEMENTS**

I would like to express my deepest and sincere gratitude to my supervisor, Assoc. Prof. Dr. Zuhailawati Bt Hussain for her supervision, advice, guidance and encouragement throughout my research project to make this work successful. I also would like to extend my sincere gratitude to my co-supervisor, Dr. Anasyida Bt Abu Seman @ Hj Ahmad, who has given me a very helpful advice and valuable comments on writing of this thesis.

My special thanks to AUN/Seed-net program for their generosity on giving me this opportunity and financial support to pursue my master's degree.

I would like to convey my special thanks to Dean, Deputy Dean, lectures and all staffs of School of Materials and Mineral Resources Engineering (SMMRE) for their kind assistants and supports. Many thanks to Universiti Sains Malaysia (USM) and SMMRE for research facilities.

I owe my loving thanks to my parents, wife, sisters, brothers and Dr. Tran Duc Huy for their encouragement and understanding. Special thanks to all my friends in SMMRE for their supports.

## TABLE OF CONTENTS

ACKNOWLEDGEMENTS .....	II
TABLE OF CONTENTS .....	III
LIST OF TABLES .....	VII
LIST OF FIGURES .....	VIII
LIST OF ABBREVIATION .....	XIV
ABSTRAK .....	XV
ABSTRACT .....	XVII
CHAPTER 1 INTRODUCTION .....	1
1.1 Research Background.....	1
1.2 Problem Statement .....	4
1.3 Objective.....	6
1.4 Scope of work .....	6
CHAPTER 2 LITERATURE REVIEW .....	8
2.1 Introduction to Aluminum Alloy .....	8
2.2 Aluminum alloy A356.....	9
2.3 General Solidification Aspects of Al-Si Alloy .....	11
2.4 Semi-solid Metal (SSM) Processing .....	15
2.4.1 Introduction of Semi-Solid Metal Processing .....	15
2.4.1.1 Thixocasting .....	18
2.4.1.2 Rheocasting .....	21
2.4.2 Cooling Slope Casting Process.....	24
2.4.2.1 Effect of Casting Factor of Cooling Slope on Microstructure of Slurry	

2.4.3	Formation of Particles During Semisolid Casting .....	28
2.4.3.1	Dendrite Fragmentation Mechanism .....	28
2.4.3.2	Copious Nucleation Mechanism.....	29
2.5	Severe Plastic Deformation (SPD).....	31
2.5.1	Introduction .....	31
2.5.2	Ultrafine Grained (UFG) Material.....	32
2.5.3	Equal Channel Angular Pressing.....	32
2.6.4	Shearing Characteristics Associated with ECAP .....	34
2.6.5	Grain refinement by ECAP .....	39
2.7.2	Wear Mechanism .....	44
2.7.2.1	Adhesive Wear .....	44
2.7.2.2	Delamination Wear .....	45
2.7.2.3	Abrasive Wear .....	45
2.7.2.4	Oxidation Wear .....	46
CHAPTER 3 MATERIALS AND METHODOLOGY.....		47
3.1	Introduction.....	47
3.2	Raw Material.....	49
3.3	X-Ray Fluorescence Analysis of Aluminum Alloy Ingot .....	49
3.4	Mixing of Al-Si-Mg Alloy Ingot .....	50
3.4.1	Differential Scanning Calorimetry Analysis .....	50
3.5	Casting Experiments .....	51
3.5.1	Conventional Casting.....	51
3.5.2	Cooling Slope Casting .....	52
3.6	Characterization of Cast Alloy.....	54
3.6.1	Optical Microstructure .....	54

3.6.2	Vickers Hardness Measurement .....	55
3.7	Preparation of Feed Material for Equal Channel Angular Pressing (ECAP) ..	56
3.7.1	Cutting and Machining .....	57
3.7.2	Annealing .....	57
3.8	Equal Channel Angular Pressing (ECAP).....	58
3.9	Characterization of ECAPed Al-7Si-Mg Alloy .....	60
3.9.1	Optical Microscope.....	60
3.9.2	Hardness Measurement .....	61
3.9.3	X-ray Diffraction (XRD) .....	61
3.9.4	Wear Test After ECAP .....	62
3.9.5	SEM and EDX Analysis .....	64
CHAPTER 4 RESULTS AND DISCUSSION .....		65
4.1	Introduction.....	65
4.2	X-rays Fluorescence (XRF) Analysis of Al-7Si-Mg Alloy.....	65
4.3	Analysis of Al -7Si-Mg Alloy by Differential Scanning Calorimetry (DSC)	66
4.4	Cooling Slope Casting.....	67
4.5	Effect of the Pouring Temperature on the Microstructure of Cooling Slope Cast Al-7Si-Mg Alloy.....	73
4.5.1	Microstructure Observation.....	73
4.5.2	Hardness.....	76
4.6	Effect of Slope Length on Microstructure of Cast Alloy .....	77
4.6.1	Microstructure observation .....	77
4.6.2	Hardness.....	80
4.7	Effect of Cooling Slope Temperature on Microstructure of Cast Alloy .....	81
4.7.1	Microstructure Observation.....	81

4.7.2	Hardness.....	84
4.8	Annealing.....	84
4.8.1	Microstructure Observation of Annealed Alloy.....	85
4.8.2	Vickers Hardness of As-cast Samples and As-annealed Samples.....	87
4.9	Effect of Equal Channel Angular Pressing processing.....	88
4.9.1	Microstructure observation.....	88
4.9.2	Hardness.....	92
4.9.3	X-ray Diffraction Analysis.....	93
4.10	Wear Resistance Properties.....	96
4.10.1	Wear Response.....	97
4.10.2	Friction Coefficient.....	100
4.10.3	Worn Surface Morphology.....	103
CHAPTER 5 CONCLUSIONS AND FUTURE RECOMMENDATION.....		110
5.1	Conclusions.....	110
5.2	Future Works.....	112
REFERENCES.....		113
PUBLICATIONS.....		121
APPENDICES.....		122
APPENDIX A.....		122
APPENDIX B.....		122

## LIST OF TABLES

		<b>Page</b>
Table 2.1	Composition of standard aluminum alloy A356 (Warmuzek and Malgorzata, 2004)	10
Table 2.2	Definition of the rotation in different routes (Furukawa et al., 1998)	38
Table 2.3	Schematics of the deformation of a unit element after n passages through the die (Furukawa et al., 1998)	38
Table 3.1	List of experiments to investigate the effect of pouring temperature	54
Table 3.2	List of experiments to investigate the effect of slope length	54
Table 3.3	List of experiments to investigate the effect of slope temperature	54
Table 3.4	Sample name with parameters investigated for ECAP experiments	59
Table 4.1	Composition of Al-Si-Mg alloy ingot	66
Table 4.2	Composition of Al-7Si-Mg alloy	66
Table 4.3	Grain size analysis of conventional and cooling slope cast alloy in centre zone	70
Table 4.4	Grain size analysis of cooling slope cast alloy in centre zone at different pouring temperature	74
Table 4.5	Grain size analysis of cooling slope cast alloy in centre zone at different cooling slope lengths and different pouring temperatures	78
Table 4.6	Grain size analysis of cooling slope cast alloy in centre zone at different slope temperatures and different pouring temperatures	82
Table 4.7	Crystallite size of aluminum alloy before and after ECAP processing with different route and different casting process	94

## LIST OF FIGURES

		<b>Page</b>
Figure 2.1	Equilibrium binary phase diagram aluminum – silicon alloy (Mondolfo, 1976)	10
Figure 2.2	Microstructures of aluminum alloy A356. (a) and (b) as-cast alloy; (c) and (d) as-annealed alloy (Cepeda-Jimenez et al., 2011)	11
Figure 2.3	Schematic of Al-Si phase diagram indicating (1) pure metals, (2) solid-solution alloys, (3) hypoeutectic alloys, (4) eutectic alloys, (5) hypereutectic alloys, (6) liquid metal, (7) semisolid metal (Kurz and Fisher, 1989)	12
Figure 2.4	Concentration and temperature fields of columnar and equiaxed dendrites, showing actual temperature gradient $T_q$ and liquidus temperature $T_L$ near the solid-liquid interface, and resulting region on constitutional undercooling (shaded) at the dendrite tips (Kurz and Fisher, 1989)	14
Figure 2.5	Schematic of the Couette-type viscometer (Lashkari and Ghomashchi, 2007)	15
Figure 2.6	(a) Dendritic structure (quenched at 0.36 fraction solid) result from shearing after partial solidification; (b) Non-dendritic structure (quenched at 0.6 fraction solid) resulting from shearing before solidification begins (Alloy: Sn-15%Pb) (Flemings, 1991)	16
Figure 2.7	Schematic of the two semi-solid processing approaches (De Figueredo, 2001)	18
Figure 2.8	Temperature versus time for thixocasting process (Legoretta et al., 2008)	19
Figure 2.9	(a) Schematic of MHD process (Hirt and Kopp, 2009); (b) SSM microstructure obtained using the MHD process. Alloy: A356 (De Figueredo, 2001)	20
Figure 2.10	Temperature versus time for rheocasting process (Legoretta et al., 2007)	21

Figure 2.11	Schematic illustration of the stages of New Rheocasting (NRC) (Adachi et al., 2004)	22
Figure 2.12	(a) Schematic of the SSR process, (b) typical thermal history of SSR process (Flemings et al., 2003)	23
Figure 2.13	Microstructure of slurry produced using SSR. Alloy A356 (Flemings et al., 2003)	24
Figure 2.14	Schematic illustrate thixocasting process using cooling slope (Haga and Kapranos, 2002a)	25
Figure 2.15	Schematic illustrate rheocasting using cooling slope (Haga and Kapranos, 2002b)	25
Figure 2.16	Microstructure of cooling slope casting: (a) at pouring temperature of 620°C; (b) at pouring temperature of 650°C (Haga and Kapranos, 2002b)	27
Figure 2.17	(a) Schematic of dendrite multiplication; (b) schematic illustration of evolution of structure during solidification with vigorous agitation (Flemings et al., 2004)	28
Figure 2.18	(a) schematic illustration of the mechanism of necking and detachment of nuclei from the surface of the cooling slope; (b) Temperature profiles in the liquid in the solidification front, for an alloy with partition coefficient $K < 1$ . $\Delta T$ , undercooling temperature; $V_g$ , growth rate (Rosso, 2012)	30
Figure 2.19	Schematic illustration of the ECAP process (Furukawa et al., 2001)	33
Figure 2.20	Schematic illustrations of different processing routes (Stolyarov et al., 2001)	34
Figure 2.21	Schematic illustration of shearing in a single pressing through the die: X, Y, and Z define three orthogonal planes of observation (Furukawa et al., 1998)	35
Figure 2.22	Schematic illustration of shearing after two passes without rotation (route A) (Furukawa et al., 1998)	35

Figure 2.23	Schematic illustration of shearing after two passes with rotation of 90° (route BC) (Furukawa et al., 1998)	36
Figure 2.24	Schematic illustration of shearing after two passes with rotation of 180° (route C) (Furukawa et al., 1998)	36
Figure 2.25	Grain structure after 1 pass (the planes is denoted as X, Y, and Z which is the same as in Figure 2.20 (Iwahashi et al., 1998)	39
Figure 2.26	Shearing patterns associated with ECAP through route A, BC, and C, respectively (Iwahashi et al., 1998)	41
Figure 2.27	Microstructure after 3 passes with route BC (Iwahashi et al., 1998)	41
Figure 2.28	Spot spreading from selected area electron diffraction (SAED) patterns describing the angle of misorientation between the grains. Route B has the most equiaxed grain structure (Iwahashi et al., 1998)	42
Figure 2.29	Schematic of adhesive wear (Kopeliovich, 2014)	44
Figure 2.30	Schematic of Abrasive wear: (a) three-body abrasive wear; (b) two-body abrasive wear (Kopeliovich, 2014)	46
Figure 3.1	Flow chart of experimental procedure	48
Figure 3.2	Conventional casting with bottom pouring from crucible	52
Figure 3.3	The schematic of the cooling slope casting with bottom pouring from the crucible	53
Figure 3.4	Section of sample and position of observing microstructure	55
Figure 3.5	(a) Sample before and after cutting process; (b) machining process	57
Figure 3.6	Temperature – Time profile of annealing process for cast samples	58
Figure 3.7	Schematic illustration of the ECAP process	58

Figure 3.8	Process of a 120° ECAP die and corresponding microstructural planes investigated	60
Figure 3.9	Schematic sectioning of ECAPed Al-7.5Si-Mg alloy rod	61
Figure 3.10	Principle diagram of pin on disc wear and friction monitor	62
Figure 4.1	DSC curve of Al-7Si-Mg alloy recorded during cooling from the molten state	67
Figure 4.2	Microstructure of a sample cast directly into a vertical cold mild steel mould at pouring temperature of 640°C: (a) thin wall zone, (b) middle zone and (c) the centre zone	69
Figure 4.3	Microstructure of a sample cast via the cooling slope into a vertical cold mild steel mould at a pouring temperature of 640°C; cooling slope length of 250 mm; cooling slope at room temperature; tilt angle of 60°: (a) the thin wall zone, (b) the middle zone and (c) the centre zone	70
Figure 4.4	Microstructure of remnant Al-7Si-Mg alloy on the cooling slope titled 60° and poured at 640 °C with cooling length of 250 mm. (a) the sample at top of cooling slope; (b) the sample at middle of cooling slope; (c) the sample at bottom of cooling slope; and (d) the sample in the mould	71
Figure 4.5	Optical micrographs of samples cast via the cooling slope with varying pouring temperature, cooling length of 250mm, tilt angle of 60°, and slope held at room temperature	75
Figure 4.6	Vickers hardness of the samples that were cast by cooling slope casting with different pouring temperature	77
Figure 4.7	Optical micrographs of sample in the center zone cast via cooling slope with following pouring temperature and cooling length of: (a) 625°C – 150 mm; (b) 625°C – 250 mm; (c) 625°C – 350 mm; (d) 640°C – 150 mm; (e) 640°C – 250 mm; (f) 640°C – 350 mm; (g) 660°C – 150 mm; (h) 660°C – 250 mm; (i) 660°C – 350 mm	79
Figure 4.8	Vickers hardness of samples that were cast by cooling slope with different slope length and different pouring temperature	80

Figure 4.9	Optical micrographs of samples cast onto stainless steel cooling slope into cold steel mould with condition of process follows: Pouring temperature: 625°C, 640°C, 660°C, 680°C; Slope temperature: Room, 200°C, 400°C	83
Figure 4.10	Vickers hardness of samples that cast by cooling slope casting with different slope temperature and pouring temperature	84
Figure 4.11	Optical micrographs at two magnifications showing primary $\alpha$ -Al phase and eutectic Si particles in the Al-7Si-Mg alloy subjected to anneal: (a and b) cooling slope casting sample; (c and d) cooling slope casting annealed sample; (e and f) conventional casting sample; (g and h) conventional annealed sample	86
Figure 4.12	Vickers hardness of cooling slope (CS) and conventional cast (CC) alloys for as-cast and the as-annealed conditions	87
Figure 4.13	Optical micrographs of the samples after 4 passes ECAP by route A and Bc	90
Figure 4.14	Optical micrograph of the samples at high magnification after 4 passes of ECAP by route A and BC	91
Figure 4.15	Vickers hardness of SSM samples produced by ECAP following routes A and BC	93
Figure 4.16	XRD pattern of samples that are after anneal and after four passes ECAP by routes A and BC	94
Figure 4.17	Volume loss as a function of load for each sample at sliding distance of 5 km	98
Figure 4.18	Specific wear rate as a function of load for all samples	99
Figure 4.19	Variation of friction coefficient the conventional casting, cooling slope casting (CS), as-ECAP of conventional casting (CCE), and as-cooling slope casting ECAP (CSE) under different applied load, i.e., (a) 10N, (b) 30 N, and (c) 50N	101

Figure 4.20	Average value of friction coefficient of the CC, CCE, CS, and CSE at applied load of 10 N, 30 N and 50 N	103
Figure 4.21	SEM morphologies of worn surfaces of samples at applied loads of 10 N, 30 N and 50 N	105
Figure 4.22	BEI image of worn surface with corresponding EDX of (a) as-conventional cast (CC) sample, (b) as-cooling slope casting (CS) sample, (c) as-ECAP of conventional casting (CCE) sample and (d) as-ECAP of cooling slope casting (CSE) sample under applied load of 10N	107
Figure 4.23	BEI image of worn surface with corresponding EDX of (a) as-conventional cast (CC) sample, (b) as-cooling slope casting (CS) sample, (c) as-ECAP of conventional casting (CCE) sample and (d) as-ECAP of cooling slope casting (CSE) sample under applied load of 50N	109

## LIST OF ABBREVIATION

<b>Name</b>	<b>Abbreviation</b>
Semisolid casting	SSM
Cooling slop casting	CS
Conventional casting	CC
Equal channel angular pressing	ECAP
Severe plastic deformation	SPD
Ultrafine grain	UFG
Conventional cast ECAPed alloy	CCE
Cooling slope cast ECAPed alloy	CSE
Differential scanning calorimetry	DSC
Secondary electron scanning	SEM
X-ray diffraction	XRD
X-ray fluorescence	XRF
High pressure torsion	HPT
Accumulative Roll-Bonding	ARB
Twisted Extrusion	TE

# **KESAN UBAHBENTUK SEKUNDER KE ATAS MIKROSTRUKTUR DAN SIFAT MEKANIKAL ALOI TUANGAN Al-Si-Mg**

## **ABSTRAK**

Penyelidikan ini bertujuan mengkaji mikrostruktur dan kekerasan aloi Al-7.5Si-Mg di bawah keadaan penuangan cerun pendinginan yang berbeza dan penekanan sudut salur sama (ECAP). Kesan kaedah penuangan cerun pendinginan dengan pemboleh ubah yang berbeza seperti suhu pencurahan ( $625^{\circ}\text{C}$  –  $640^{\circ}\text{C}$  –  $660^{\circ}\text{C}$  –  $680^{\circ}\text{C}$ ), panjang cerun pendinginan (150 mm – 250 mm – 350 mm), suhu cerun pendinginan (suhu bilik –  $200^{\circ}\text{C}$  –  $400^{\circ}\text{C}$ ) dan kaedah penuangan konvensional telah dibentangkan. Aloi tuangan dan aloi ECAP dinilai untuk mikrostruktur, kekerasan, corak pembelauan Sinar-X, rintangan haus, mikroskop imbasan electron dan Sina-X serakan tenaga. Mikrostruktur bagi aloi tuangan konvensional pada suhu pencurahan  $640^{\circ}\text{C}$  adalah kasar dan menyerupai dendrit. Walaubagaimanapun, mikrostruktur yang seragam, halus dan globul telah diperoleh melalui penuangan cerun pendinginan dengan suhu pencurahan pada  $625^{\circ}\text{C}$  –  $660^{\circ}\text{C}$ , panjang cerun pendinginan pada 150 mm – 350 mm dan suhu pencerunan pada suhu bilik hingga  $200^{\circ}\text{C}$ . Hal ini dijelaskan oleh penukleusan yang banyak berlaku pada permukaan cerun dan nukleus tersebut kemudiannya tertanggal disebabkan daya olakan semasa proses pencurahan. Leburan logam yang mempunyai dendrit  $\alpha\text{-Al}$  sama dimensi yang tinggi terkumpul di dalam acuan sebaik sahaja pendinginan pantas berlaku maka mikrostruktur globular halus terhasil. Mikrostruktur bagi aloi tuangan cerun pendinginan lebih halus dengan taburan jujuk mikrostruktur yang seragam berbanding aloi tuangan konvensional, selepas melalui ECAP sama ada laluan A atau Bc. Hal ini menyumbang kepada kekerasan aloi tuangan pendinginan (84Hv) yang lebih tinggi daripada aloi tuangan konvensional (76Hv). Rintangan haus bagi kedua-dua aloi tuangan meningkat selepas ECAP.

Namun, peningkatan tersebut lebih signifikan bagi aloi tuangan cerun pendinginan kerana mikrostrukturnya yang lebih halus dan taburan jujuk mikrostruktur yang homogen, dan juga kekerasan yang lebih tinggi.

# **EFFECT OF SECONDARY PLASTIC DEFORMATION ON THE MICROSTRUCTURES AND MECHANICAL PROPERTIES OF CAST Al-7Si-Mg ALLOY**

## **ABSTRACT**

The purpose of this research is to study microstructure and hardness of Al-7Si-Mg alloy under different cooling slope casting conditions and equal channel angular pressing (ECAP). The effect of cooling slope casting method with varying variables, such as pouring temperature (625°C – 640°C – 660°C – 680°C), cooling slope length (150 mm – 250 mm– 350 mm) and cooling slope temperature (room temperature – 200°C – 400°C) and conventional casting method are investigated. The as-cast alloys and as-ECAPed alloys were analyzed based on Differential Scanning Calorimetry, X-ray fluorescence, microstructures, hardness, X-ray Diffraction pattern, wear resistance, Secondary Electron Microscope and Energy Dispersive X-ray. Microstructure of conventional cast alloy cast at pouring temperature of 640°C was coarse and almost dendrite the structure. However, uniform, fine and globular microstructure could be obtained from cooling slope casting with pouring temperature range of 625°C – 660°C, cooling slope length range of 150 mm – 350 mm and slope temperature ranging from room temperature to 200°C. This is due to copious nucleation occurred on slope surface and these nuclei were then detached due to the force convection during pouring process. The molten metal with high content of fine equiaxed  $\alpha$ -Al dendrites was collected in the mould and once rapid cooling took place, fine globular microstructure was formed. Microstructure of cooling slope cast alloy after ECAP subjected to either by route A or B<sub>c</sub> was finer with homogeneous distribution of microstructure

constituents than that of conventional cast alloy, which contribute to higher hardness of cooling cast alloy (84Hv) compared to conventional cast alloy (76Hv). The wear resistance was improved after ECAP both cast alloys but the improvement was significantly high for cooling slope casting alloy due to finer and homogenous distribution of microstructure constituents and higher hardness.

# CHAPTER 1

## INTRODUCTION

### 1.1 Research Background

Aluminum alloys have been widely used in the automotive and aerospace industries, as the trend nowadays is to achieve higher performance without increasing the weight. Therefore, more and more automotive components are made of aluminum alloys in order to reduce the weight, at the same time maintaining or improving mechanical properties. Apart from their excellent casting characteristics, wear and corrosion resistance, aluminum-silicon casting alloys are used extensively because they also impart a wide range of mechanical properties and high strength to weight ratio. The increasing demand and use of these aluminum cast alloys have promoted a lot of researches and developments to enhance the casting and mechanical properties. Among these research and development, semisolid casting and severe plastic deformation techniques have recently applied in order to improve mechanical properties of aluminum alloys (Tsai et al., 2009).

Semi-solid metal (SSM) processing was first discovered in the early 1970s, when Flemings and co-workers studied the flow behavior of metals in a semi-solid state (Omar et al., 2009). Since SSM was discovered, many semi-solid methods have been developed. Among these methods, cooling slope casting method is an attractive method as it is a very simple process with very low equipment and running costs. In cooling slope process, the semi-solid metal was made by a simple process of pouring the slightly preheated melt down a cooling slope and subsequent solidification in a die. The principle of cooling slope casting is that the copious nucleation of primary

phase on the cooling slope coupled with low force convection due to pouring process can result in the formation of uniform, fine and globular microstructure, which contributes to high mechanical properties of material (Wang et al., 2011). Cooling slope method has been proven to be highly effective for manufacture of high quality semisolid feedstock under both thixocasting and rheocasting conditions (Hirt and Kopp, 2009). Some of important operational parameters in cooling slope casting are pouring temperature, cooling slope length and slope temperature which affect the nucleation of primary phase on the cooling slope surface. The survival of these nuclei during pouring of the molten metal into the mould, results in the different microstructure of alloy (Legoretta et al., 2008).

On the other hand, severe plastic deformation (SPD), which refines grain size and introduces nano-scale features in metals and alloys, offers a new prospect of enhancing metal properties beyond the levels otherwise attainable. Among SPD techniques, equal channel angular pressing (ECAP) is the most favorable SPD technique because it can be used to produce bulk ultra fine grain (UFG) materials without changing its cross-sectional area and shape as compared to other SPD techniques (Valiev et al., 2006). The principle of ECAP is that a billet with square or circular cross-section is pressed through a die having two channels of equal cross-section areas and with the channels inclined at an angle with respect to each other. The billet undergoes simple shear deformation at the die channel intersection, and the strain imposed in a single pass depends on the angle between the channels, radius curvature at the outer corner of the die intersection, and the friction conditions prevailing between the die and billet (Segal, 2003). The repetitive pressing operations are performed on billet, resulting in large cumulative strains.

Furthermore, as demonstrated by Swaminathan et al. (2008) the strain routes can be varied by the rotation of billet after each passes in repetitive ECAP, which has led to either a monotonic increase in strain during a succession of passes (route A or B<sub>A</sub>) or a redundant straining after certain number of passes (route B<sub>C</sub> or C).

ECAP technique has been investigated to improve mechanical properties of Al-Si alloys. Typically a feed material of as-cast Al-Si alloy, which is produced by conventional casting, is used with hypoeutectic solidification structure, consisting of  $\alpha$ -Al primary dendrites and interdendritic network of lamellar eutectic silicon (Moradi et al., 2009; Gutierrez-Urrutia et al., 2007). That is why the distribution of the eutectic constituent during the ECAP processing become inhomogeneous, which has not improved the ductility of hypoeutectic aluminum alloys (Garcia-Infanta et al., 2008a). On the other hand, uniform, fine and globular microstructure of alloy can be produced by semisolid casting process (Atkinson, 2007). The uniform, fine and globular microstructure of Al-Si alloy is one of considerable factor in obtaining homogenous microstructure in distribution of  $\alpha$ -Al primary phase and eutectic constituent after ECAP which would contribute to higher ductility and higher mechanical properties.

In this study, the cooling slope was used to investigate the effect of cooling slope on microstructure evolution with an aim to achieve fine and globular microstructure. The cast alloy was then subjected to ECAP in order to evaluate the effect of ECAP on the properties of Al-Si-Mg alloy with the uniform, fine and globular microstructure.

## 1.2 Problem Statement

Among aluminum alloys, Al-Si-Mg alloy has been widely used in the automotive, aerospace and electronic industry because of its excellent castability, low thermal expansion coefficient, low density, good wear resistance, and high strength at elevated temperature (Gutierrez-Urrutia et al., 2007). However, low ductility and toughness of Al-Si-Mg alloy limits its uses in applications where these properties are not important. Various methods have been used to improve the mechanical properties by changing solidification conditions, using additional heat treatments or introducing alloying elements to refine the primary  $\alpha$ -Al phase and to modify the Si particle morphology (Timpel et al., 2012). But, appreciating all the economic drawbacks of alloying or heat treatment methods, the possibility of applying any other technique to refine the primary  $\alpha$ -Al phase and to disperse the Si particles in Al-Si-Mg alloy is highly demanded to improve mechanical properties.

Semisolid casting process has been reported to be used to produce Al-Si alloy with uniform, fine and globular microstructure and with less porosities and shrinkages, resulting in the mechanical improvement (Atkinson, 2007; Rosso, 2012). Cooling slope casting process is one of semisolid casting methods having very low equipment, running cost and simple process (Biol, 2007). Therefore, cooling slope was used to investigate with the aim to produce cast aluminum alloy with uniform, fine and globular microstructure.

ECAP process is a good candidate that could be used to achieve a free porosity and the ultrafine grain aluminum alloy which would contribute to higher mechanical properties as compared with as-cast alloy. Although some papers have reported the

ECAP processing for Al-Si-Mg alloy, all of them have focused on the effect of ECAP processing routes to microstructure and mechanical properties of as-conventional cast Al-Si-Mg alloys that have the microstructure consisting of coarse primary aluminum dendrites and interdendritic network of lamellar eutectic silicon. As a result of coarse primary aluminum dendrites and interdendritic network of lamellar eutectic silicon, the formation of inhomogeneous distribution of primary  $\alpha$ -Al phase and Si particles after ECAP have been reported (Cepeda-Jimenez et al., 2011; Moradi et al., 2009; Garcia-Infanta et al., 2008a; Garcia-Infanta et al., 2008b; Gutierrez-Urrutia et al., 2007). Therefore, the mechanical properties of Al-Si alloy are not significantly improved after ECAP.

To overcome the above problem, it is believed that with uniform, fine and globular microstructure which could be achieved by using semi-solid casting is more suitable as a feedstock for ECAP. With the homogenous distribution of microstructure constituents, the mechanical properties of Al-Si-Mg alloy are expected to be significantly improved. However, as far as published literature concern, there seems to be no research conducting ECAP process using semisolid cast alloy as the feed material.

The mechanical properties of the resultant deformed alloy are still opened for further investigation especially while the alloy is exposed to load during its service. In practical applications, most of machine components involve relative motion incorporating with friction and wear. The wear properties of engineering materials have significant effects on the service-ability and durability of components. As a result, the wear properties must be counted into account in the design of engineering

component (Gao et al., 2012). Therefore, the wear resistance of semisolid casting and ECAPed Al-Si-Mg were investigated in this work.

### **1.3 Objective**

The primary objectives of this work are:

1. To study the microstructure and hardness of Al-Si-Mg under different cooling slope casting conditions.
2. To study the effect of ECAP on the microstructure, hardness and grain refinement of Al-Si-Mg cooling slope cast alloy.
3. To study wear behavior of Al-Si-Mg alloy process by cooling slope casting and ECAP.

### **1.4 Scope of work**

The present research includes: Al-7Si-Mg alloy preparation, conventional and cooling slope casting experiment, and equal channel angular pressing (ECAP) process experiment. The first stage, the Al-7Si-Mg alloy was produced by mixing Al-Si-Mg alloy ingot with pure Al and pure Mg. The second stage, the Al-7Si-Mg alloy was cast with a cooling slope denoted cooling slope casting and without the cooling slope denoted conventional casting. Effect of various cooling slope casting parameters on microstructure and hardness of cast alloy i.e., pouring temperature (625°C-680°C), cooling slope length (150 mm-350 mm) and slope temperature (room temperature – 400°C) was investigated. The third stage, ECAP process was used to further enhance properties of both cast alloys (conventional and cooling slope cast alloy). Cast alloy was prepared on rod shape and annealed and then subjected to ECAP process

following route A and Bc. The properties of ECAPed alloys such as microstructure, hardness, and wear resistance were studied.

## **CHAPTER 2**

### **LITERATURE REVIEW**

#### **2.1 Introduction to Aluminum Alloy**

A number of unique and attractive properties account for the engineering significance of aluminum alloy, including light weight, good mechanical properties, high specific strength, excellent corrosion resistance (DeGarmo et al., 2011). In addition, with the current demand of weight reduction for improved product performance and fuel economy, aluminum alloys are increasingly being used in critical structural applications in electronic, automotive and aerospace industries (Jamaati et al., 2011). The development of aluminum alloy began when the properties of the unalloyed metals were evidently insufficient to meet the need of potential customer. Thus alloying elements are added to produce sufficient properties for the applications (ASM Handbook, 1993).

To date, many aluminum alloys were purposely designed for specifications and properties of aluminum and its alloys by standard of four digit numeric code (DeGarmo et al., 2011). These codes are of Aluminum Association System and are widely used. This standard classifies aluminum alloys into cast and wrought. The codes are separated and slightly different for cast and wrought alloys. In this study, cast aluminum alloy is used. The designations for cast aluminum alloys are shown in Appendix A.

## 2.2 Aluminum alloy A356

Aluminum alloy A356 which is one of Al-Si alloys is widely used in casting industry, especially in the automotive industry due to its excellent fluidity during casting, high strength to weight ratio, low thermal expansion coefficient, and heat treatability (Tsai et al., 2009). The strength, ductility, and castability of this alloy can be improved by modification of eutectic silicon and primary  $\alpha$ -Al phase either by rapid solidification or by the introduction of modifiers to the melt (Zuo et al., 2009). The elements lanthanum, cerium, arsenic, antimony, selenium, and cadmium have been reported to stimulate a silicon modification effect, but in commercial application only sodium, strontium, and antimony are used (Timpel et al., 2012). Master alloys Al-Ti-B was used in commercial application to refine the primary  $\alpha$ -Al phase as well (Biol, 2009). The small amount of magnesium in this alloy has a significant role that enables it to have heat treatment ability to increase the mechanical properties of the alloys (Kaufman and Rooy, 2004; Hirt and Kopp, 2009).

Most of the applications of semi-solid casting processes are used for the production of Al-Si-Mg alloys such as A356 alloy because of the wide processing window for semi-solid forming and high strength and ductility it offers (Wannasin et al., 2008). The standard aluminum alloy A356 has composition as shown in Table 2.3 and its phase diagram is shown in Figure 2.1. The phase diagram has shown 0 wt% to 25 wt% of silicon (Si). Referring to the phase diagram, the aluminum alloy with content of Si around 7wt% has the microstructure which consists of primary  $\alpha$ -Al phase and eutectic phase.

**Table 2.1:** Composition of standard aluminum alloy A356 (Warmuzek and Malgorzata, 2004)

Alloy	Chemical composition (main components), wt%						
Designation	Si	Cu	Mg	Mn	Ni	Fe	Al
A356	6.5-7.5	0.25max	0.2-0.45	0.35max	...	0.6max	balance

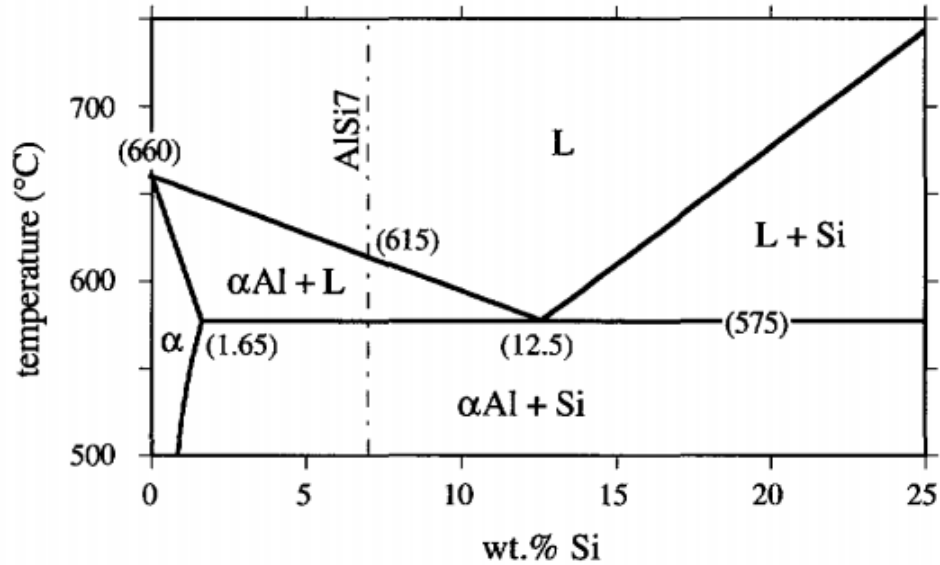


**Figure 2.1:** Equilibrium binary phase diagram aluminum – silicon alloy (Mondolfo, 1976)

The microstructure of aluminum alloy A356 has been shown in a lot of articles and books as shown in Figure 2.2. The microstructure of this alloy mainly consists of primary  $\alpha$ -Al phase and interdendritic eutectic phase. The morphology of Si phase became coarser and more globular after annealing (Figure 2.2 d).

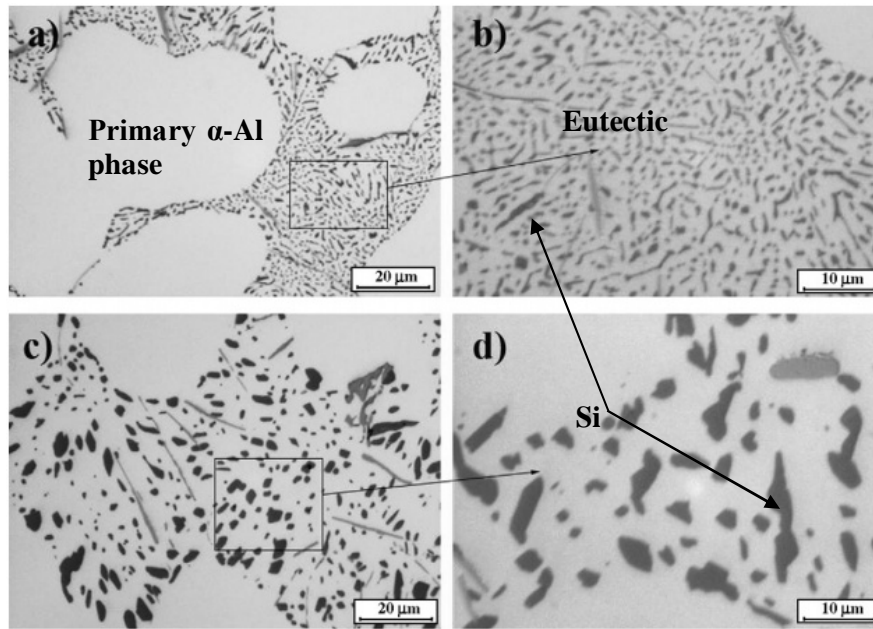


**Figure 2.2:** Microstructures of aluminum alloy A356. (a) and (b) as-cast alloy; (c) and (d) as-annealed alloy (Cepeda-Jimenez et al., 2011)

### 2.3 General Solidification Aspects of Al-Si Alloy

Microstructure and properties of solidified Al-Si alloy are strongly dependent on alloy composition and solidification conditions. Under conventional casting conditions usually only two morphologies have to be regarded: dendrites and eutectic as described by Kurz and Fisher (1989) for a binary alloy. Dendrites are branched, tree-like crystals; eutectics are two or more phases growing simultaneously from a liquid in a fibrous or lamellar manner. The microstructure of Al-Si alloys after solidification can be divided into five types according to silicon content as showed in Figure 2.3. One can distinguish: 1, pure Al; 2, solid-solution Al(Si) alloys; 3, hypoeutectic alloys ; 4, eutectic alloy; and 5, hypereutectic alloys.

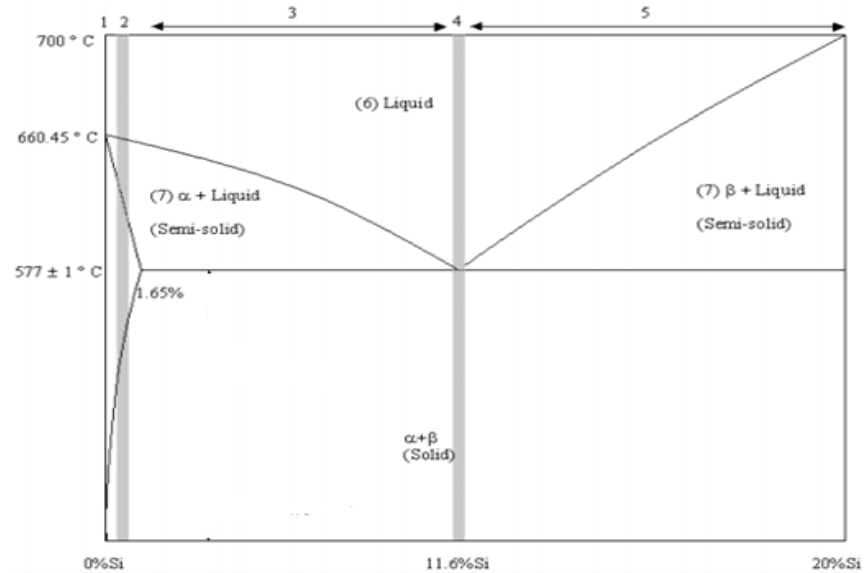


**Figure 2.3:** Schematic of Al-Si phase diagram indicating (1) pure metals, (2) solid-solution alloys, (3) hypoeutectic alloys, (4) eutectic alloys, (5) hypereutectic alloys, (6) liquid metal, (7) semisolid metal (Kurz and Fisher, 1989)

A hypoeutectic Al-Si alloy is used in this research. When a hypoeutectic solidify from liquid, the primary  $\alpha$ -Al phase forms in the semisolid region ( $\alpha + \text{liquid}$ ) as shown in Figure 2.3. The primary phase solidifies following a mechanism involving two principle stages: nucleation and growth (Kurz and Fisher, 1989).

The first stage of solidification is nucleation. The nucleus is simple unit of the appropriate crystal lattice structure for metal with atoms arranged accordingly. As liquid changes phase into solid, heat must be lost in the process. Spontaneous nucleation, known as homogenous nucleation, may occur when an alloy is cooled rapidly to a temperature well below its equilibrium freezing temperature. Undercooling is the temperature drop below the equilibrium freezing temperature at which, in practice, a metal begins to solidify (Kurz and Fisher, 1989). Due to the moderate cooling rates experienced in most metal solidification processes, the undercooling is generally not large enough for obtaining homogeneous nucleation.

Instead, solidification is commonly occurred by heterogeneous nucleation which can originate from nucleation sites at a mould wall or from solid impurities suspended in the molten metal.

The second stage of solidification is the growth of nuclei. The nuclei are formed and subsequently can grow out in either a constrained manner (from a chill wall) (Figure 2.4a) or an unconstrained manner (within the liquid) (Figure 2.4b). Usually a difference in composition exists between liquid and solid phase. The solubility of an alloy element in the primary phase is generally lower than in liquid and therefore the liquid phase will be enriched by solute atoms at the solid-liquid interface as shown in Figure 2.4c and d. As a result of this, a solute concentration gradient is formed in liquid phase at solid-liquid interface. As the liquidus temperature is dependent on the solute concentration, the solute concentration gradient in liquid phase is reflected in a gradient of the liquidus temperature as shown in Figure 2.4e and f. As actual temperature gradient in liquid is less than the liquidus temperature gradient over a certain distance (Figure 2.4e and f), this gives rise a constitutional undercooling temperature. As a result, a planar solid-liquid interface becomes unstable and cellular perturbations form. A mushy zone is formed, consisting of both solid and liquid phases. Under normal solidification conditions, the perturbations transform into dendrites growing in a preferential crystallographic direction (which is  $\langle 100 \rangle$  for aluminum) and dendrite evolve. If dendrites grow in the opposition of the heat flux, they have a columnar appearance. If dendrites grow unconstrained in an undercooled melt, the latent heat is transferred radially and morphology of dendrite becomes equiaxed as show in Figure 2.4b.

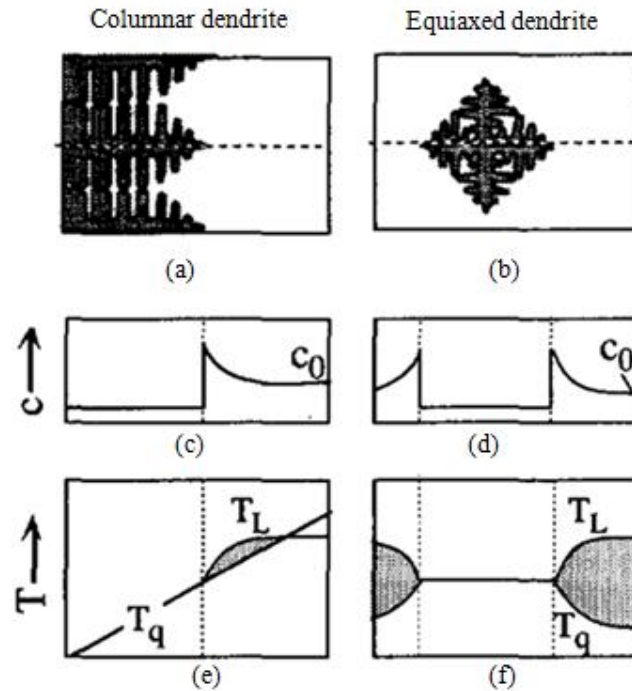


**Figure 2.4:** Concentration and temperature fields of columnar and equiaxed dendrites, showing actual temperature gradient  $T_q$  and liquidus temperature  $T_L$  near the solid-liquid interface, and resulting region on constitutional undercooling (shaded) at the dendrite tips (Kurz and Fisher, 1989)

During the course of solidification, dendrites grow and touch each others to form network of dendrite and internetwork liquid phase. The liquid phase becomes more and more enriched of solute and the composition of liquid shifts to the eutectic composition. At the end of solidification, the remaining liquid solidifies in the eutectic morphology. However, the formation of primary phase network prevents the interdendrite fluid flow, leading to formation of porosities as shrinkages in interdendrite which contribute to the reduction of mechanical properties. That is why many researches attempted to refine the dendritic primary phase and need semisolid casting methods with a number of advantages such as obtained fine, globular primary phase, leading to reduce porosities and shrinkages which contribute to the improvement of mechanical properties.

## 2.4 Semi-solid Metal (SSM) Processing

### 2.4.1 Introduction of Semi-Solid Metal Processing

Semi-solid metal (SSM) processing was first discovered by Flemings and his co-workers at the Massachusetts Institute of Technology (MIT) in the early 1970s (Omar et al., 2009). Spencer was investigating hot tearing in a Sn-15%Pb alloy through the use of a special apparatus that measured the viscosity and shear stress of solidifying as a function of fraction solid. The Couette-type viscometer consisted of two concentric cylinders with an annular space, within which the alloy was allowed to partially solidify as shown in Figure 2.5. The outer cylinder was rotated while the inner cylinder was held fixed, the material was sheared at various rates, and values for shear stress and viscosity were recorded (Flemings, 1991).

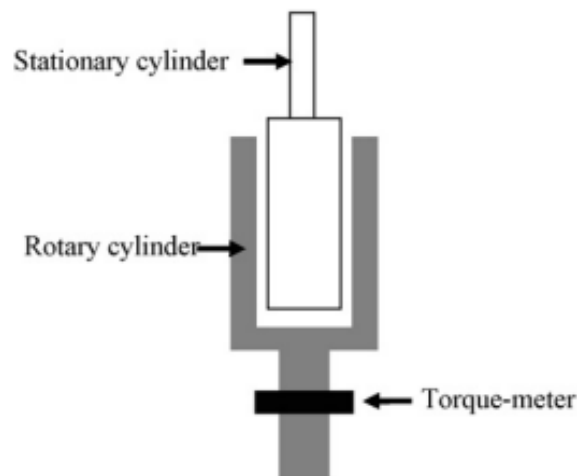


**Figure 2.5:** Schematic of the Couette-type viscometer (Lashkari and Ghomashchi, 2007)

In the course of those experiments, Spencer decided to use the same apparatus to conduct a quite different type of test. In the initial hot tearing experiments, shear was begun after the metal had solidified partially, instead of which he began the shear

above the liquidus temperature and then slowly cooled his alloy into the solidification range while it was being sheared. As a result of this slight changing experimental procedure, the results were surprising. If the alloy was sheared continuously during cooling from the fully liquid state to the semi-solid state, the shear stress was significant lower than if the alloy was cooled to semi-solid state before shear. Moreover, the non-dendritic structure was formed when continuously sheared from liquid state to semi-solid state and dendritic structure was formed when the alloy was cooled to given temperature before shear as shown Figure 2.6 (Flemings, 1991).

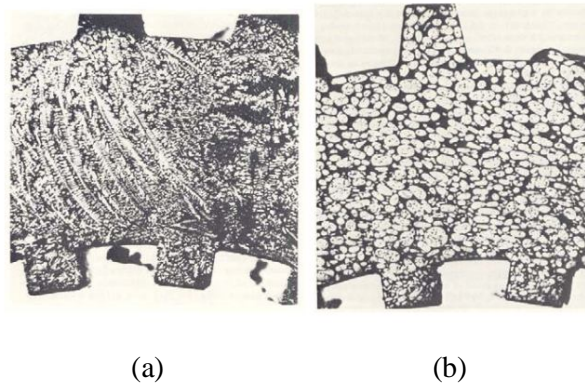


**Figure 2.6:** (a) Dendritic structure (quenched at 0.36 fraction solid) result from shearing after partial solidification; (b) Non-dendritic structure (quenched at 0.6 fraction solid) resulting from shearing before solidification begins (Alloy: Sn-15%Pb) (Flemings, 1991)

These findings had important ramification in terms of the flow behavior of semi-solid metal. At rest, non-dendritic metal slurry behaved as a rigid material in the two-phase region due to its viscosity was high enough that it could be handled as a solid. However, when shear stress was applied, the viscosity decreased dramatically, so that the material behaved more like a liquid (Atkinson, 2010). The material with non-dendrite microstructure in semi-solid state was thixotropic i.e. when it is sheared it thins and flow, when it is allowed to stand it thickens again (Salleh et al., 2013).

The benefits that semi-solid processing holds over conventional liquid metal casting is due to the flow behavior of semi-solid metal (slurry). The high viscosity of the semi-solid metal allows laminar flow during die filling to be formed and subsequently reduces part defects that could arise from gas entrapment. In addition, since semi-solid metal has lower heat content than superheat molten metal, there is less solidification shrinkage in the casting. Thus, mould can be filled more effectively and uniformly, subsequently the near net-shape is probably achieved which less post-casting machining is required (Hirt and Kopp, 2009). Moreover, the lower process temperature of semi-solid metal can be lead to a significant increase in tool life compared with conventional die casting (Jamaati et al., 2011). Furthermore, the microstructure of any component formed with semi-solid processing is fine and globular and less interdendrite porosities, which contribute to better mechanical properties of the component compared to a similar component formed from conventional casting process. This is due to increased resistance to slip provided by the increased number of grain boundaries or grain boundary area.

After the discovery by Spencer, a number of processes have been designed to utilize the advantage of the thixotropic behavior of semi-solid metallic alloy to develop a family of semi-solid metal processing techniques that could be categorized into two routes of semi-solid metal processing, i.e. two different ways to arrive at the desired point within the solid-liquid, two-phase region. The first route starts from solid state (“thixo” routes), and the second one starts from the liquid state, called “rheo” route. Figure 2.7 schematically illustrates these two routes for semi-solid metal formation (Legoretta et al., 2007).

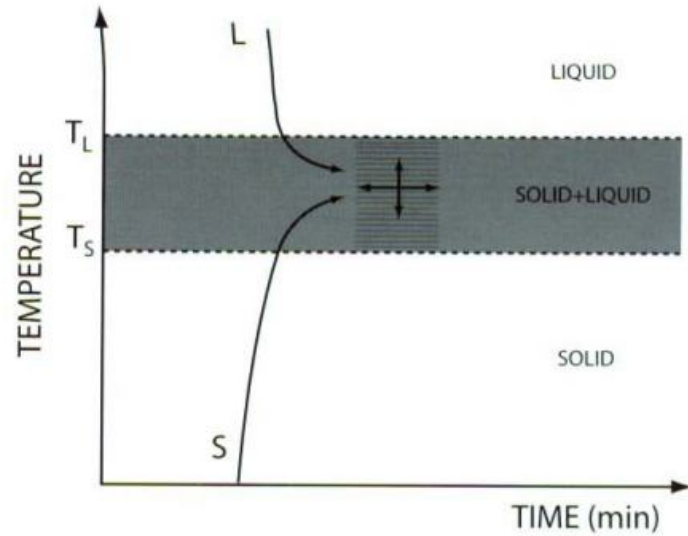
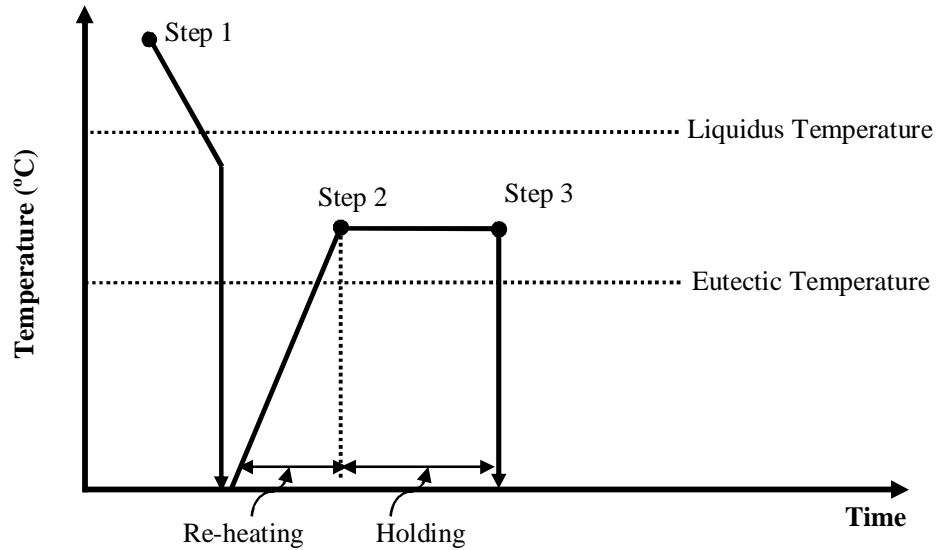


**Figure 2.7:** Schematic of the two semi-solid processing approaches (De Figueredo, 2001)

#### 2.4.1.1 Thixocasting

Thixocasting is a general term used to describe the near-net shape forming processes from partially melted, non-dendritic alloy slug within a metal die. “Thixo” processes consist in two steps and involve an intermediate solidification step as shown in Figure 2.8. In thixocasting, the material is pretreated to obtain the globular microstructure, for example by magnetic or mechanical stirring in the liquid state followed by solidification. The material with globular microstructure is then fed to the semi-solid forming process or semi-solid processing plant as a solid. Feed material is prepared, then reheated into semi-solid temperature to get the desired fraction solid, and finally cast (Rosso, 2012).



**THIXOCASTING PROCESS**

Step 1: Production of non-dendritic material

Step 2: Re-heating

Step 3: Semi-solid forming

**Figure 2.8:** Temperature versus time for thixocasting process (Legoretta et al., 2008)

During the initial years of SSM process development, the feedstock material was produced using direct mechanical stirring which was used in various ways to break up dendrites and produce thixotropic metal structures (Flemings, 1991). The combination of rapid heat extraction and vigorous melt agitation was effected by using different sizes, shapes, and velocities of stir rods. Although these methods worked well in which they effectively produced the desired metal structures, erosion of stirrer, contaminations, and entrapped gas became the weak points of the process (Atkinson, 2007).

In order to overcome the problems associated with direct mechanical stirring, a magnetohydrodynamic stirring (MHD) casting process has been developed by ITT in the USA (Kirkwood, 1994). In this technique, the solidifying melt was agitated by electromagnetic fields as shown in Figure 2.9a. Induction coils were placed around a

crucible to induce stirring forces. The crucible was equipped with a cooling system to initiate freezing in the alloy while the melt was exposed to the electromagnetic forces. Upon cooling down to ambient temperature, the alloy has a non-dendritic microstructure (Hirt and Kopp, 2009). The MHD stirring process works remarkable well and is widely used commercially (Birol, 2007). Figure 2.9b show a semi-solid microstructure typically obtained with the MHD process.

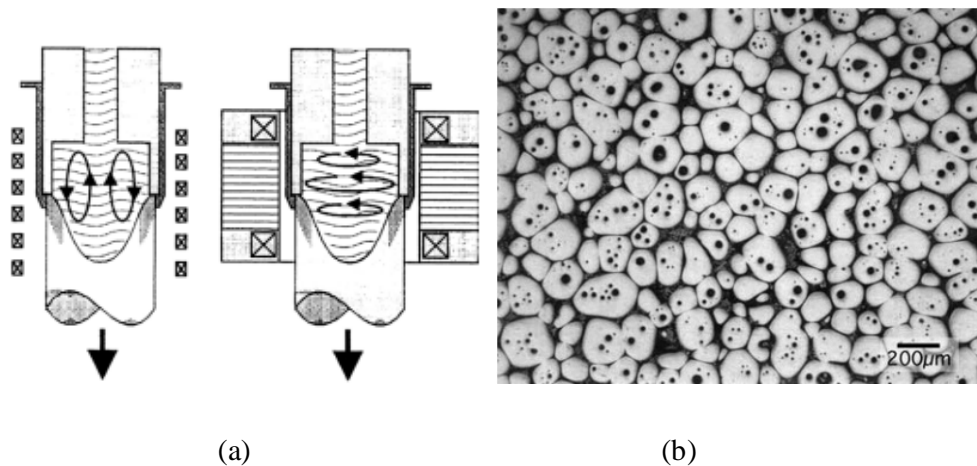
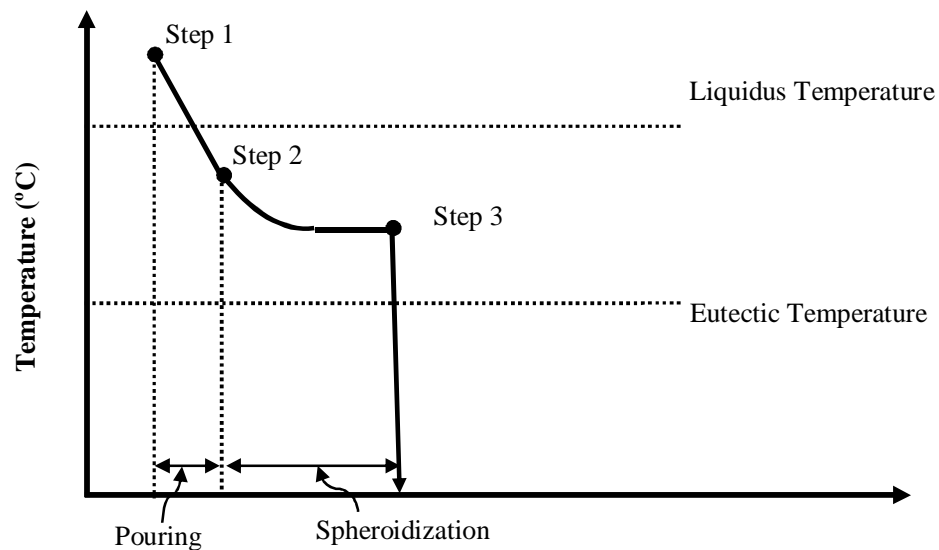


**Figure 2.9:** (a) Schematic of MHD process (Hirt and Kopp, 2009); (b) SSM microstructure obtained using the MHD process. Alloy: A356 (De Figueredo, 2001)

The thixocasting processes have many advantages. However, thixocasting processes also have some disadvantages due to the cost of intermediate step (solidification followed by reheating as shown in Figure 2.8) and the scrap produced during manufacturing has to be returned to the feedstock producer for recycling (Kaufmann et al., 2000; Hirt and Kopp, 2009). This has resulted in limitation of thixocasting but on the other hand rheocasting becoming the preferred semi-solid process (Atkinson and Liu, 2008).

### 2.4.1.2 Rheocasting

Rheocasting involves preparation of semi-solid metal slurry directly from the liquid alloy, followed by a forming process, i.e., die casting as shown in Figure 2.10. With “rheo” processes the molten metal is cooled into a semi-solid state and then is injected into a die without intermediate solidification step (Legoretta et al., 2007). Thus, overall cost of process reduces in comparison with thixocasting process (Atkinson, 2007; Hirt and Kopp, 2009).



#### RHEOCASTING PROCESS

- Step 1: Production of non-dendritic material
- Step 2: Cooling and holding for non-dendritic growth
- Step 3: Semi-solid forming

**Figure 2.10:** Temperature versus time for rheocasting process (Legoretta et al., 2007)

In the recent past, it has been discovered that one may obtain a globular microstructure without breaking up the dendritic structure (Kirkwood, 1994), but rather by creating an environment where copious nucleation can occur near the liquidus temperature of the alloy (Ping et al., 2002), and with limited growth of the formed nuclei (Van Boggelen et al., 2003). Essentially, semisolid structures develop

by controlling the nucleation and growth processes during early state of solidification. The first industrial prototype for rheocasting of aluminum component was patented by UBE.

The UBE Industries (Adachi et al., 2004), Ltd. of Japan introduced a new rheocasting process as shown in Figure 2.11, which paved the way for a new class of cost-effective, simple, and highly effective rheocasting application. In the new rheocasting process, the molten metal at near-liquidus temperature is poured onto a cooling slope or into a tilted mould to produce slurries. Nucleation occurs on the cooling slope (1(a) in Figure 2.11) or on the wall of the cup (1(b) in Figure 2.11) and then the equilibration process in the semi-solid state leads to a relatively uniform globular structure (3(a) and 3(b) in Figure 2.11). When slurries are ready for forming process, the cup is inverted, the metal drop into shot cavity, and the component is shaped.

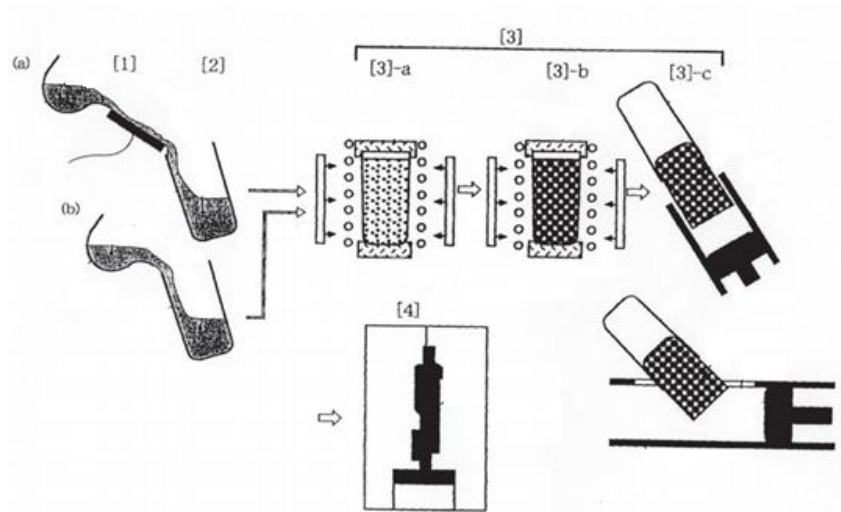


**Figure 2.11:** Schematic illustration of the stages of New Rheocasting (NRC) (Adachi et al., 2004)

Another process has been developed at MIT, which was named the Semi-Solid Rheocasting (SSR) process (Flemings et al., 2003). The three basic steps in this

process, illustrated in Figure 2.12, are as follows: (1) the melt experiences a short period of agitation as it cools through its liquidus, (2) localized heat extraction is effected by rotating cool rod (normally made of graphite), and (3) the low solid fraction slurry is cooled slowly to a desired solid fraction. The SSR process results in highly globular microstructure as shown in Figure 2.13. The cold graphite stirrer is implanted into the liquid metal, and the consequent low superheat temperature causes numerous fine dendritic grains to nucleate on the stirrer's surface. By stirring the melt, these particles are quickly removed and dispersed throughout the melt as very fine grains. These grains then remelt due to the surrounding bulk liquid that still has small areas of superheated liquid within it. Finer particles are then developed after cooling of the melt for a predefined time resulting into non-dendritic microstructures (Mohammed et al., 2013).

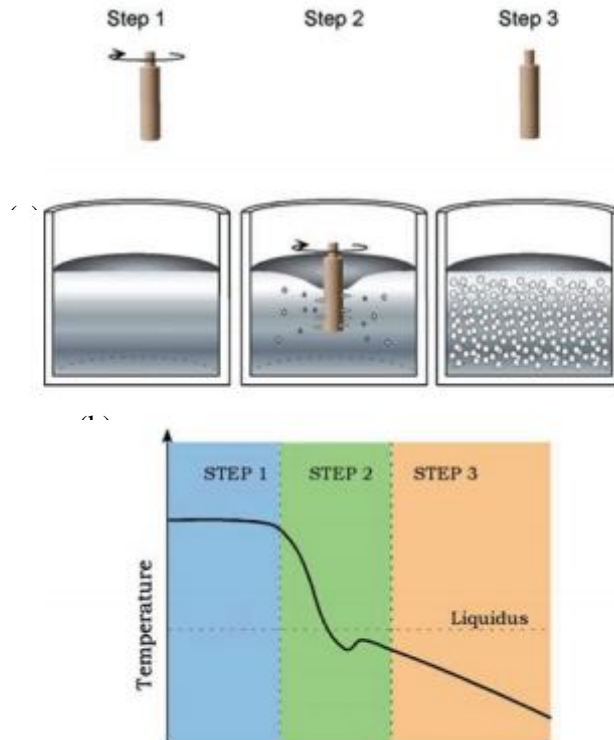


**Figure 2.12:** (a) Schematic of the SSR process, (b) typical thermal history of SSR process (Flemings et al., 2003)

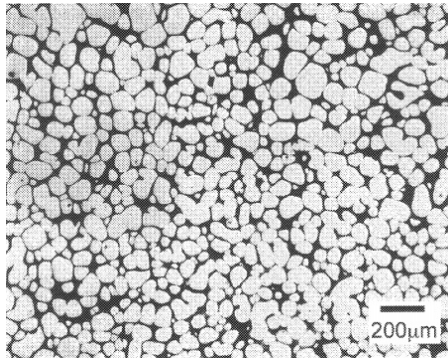


**Figure 2.13:** Microstructure of slurry produced using SSR. Alloy A356 (Flemings et al., 2003)

#### **2.4.2 Cooling Slope Casting Process**

The semi-solid casting process has a number of advantages over conventional casting process that was mentioned above, i.e. near net shaping process; improve tool life; improve mechanical properties; and especially much improved elongation (Jamaati et al., 2011; Guo et al., 2008). Thixocasting requires special feedstock materials that have globular microstructure. Typically ingots for thixocasting are continuously cast using magnetohydrodynamic (MHD) stirring, and then they are cut into appropriate size and reheated to the semi-solid state for thixocasting.

Despite of its attributes, thixocasting has not enjoyed a wide spread use due to high costs of producing special feedstock materials, limited the choice of size and the non-uniform structure of ingots from MHD casting (Biol, 2007; Haga and Kapranos, 2002a). Simple processes that have low equipment, low processing costs, and flexibility of ingot sizes are thus required to overcome these advertise. Cooling slope casting using very low equipment and running costs is an effective semisolid process introduced by Motegi, T. et al. (1998) as shown in Figure 2.14.